Hindawi
Shock and Vibration
Volume 2019, Article ID 6594345, 16 pages
https://doi.org/10.1155/2019/6594345

Research Article

Study on the Damping Mechanism of the Shrouded Blade considering Contact Features

Chaofeng Li[1,2] **Tao Li**[1] **Ruihuan Qiao**[1] **and Bangchun Wen**[1,2]

[1]*School of Mechanical Engineering & Automation, Northeastern University, Shenyang, Liaoning 110819, China*
[2]*Key Laboratory of Vibration and Control of Aero-Propulsion Systems Ministry of Education of China, Northeastern University, Shenyang, Liaoning 110819, China*

Correspondence should be addressed to Chaofeng Li; chfli@mail.neu.edu.cn

Received 9 November 2018; Revised 5 March 2019; Accepted 14 March 2019; Published 7 April 2019

Academic Editor: Hassan Haddadpour

A dynamic model of the rotating shrouded blade is established, considering the shroud mass, the Coriolis force, and the centrifugal stiffening effect. And a macroslip model of dry friction with variable normal load is established to simulate the separation-contact-stick-slip state of the shroud. The Lagrangian equation is utilized to solve the differential motion equation, and the Galerkin method is used for discretization. The influence of shroud structure's parameters such as rotational speed, contact angle, friction coefficient, clearance, and shroud position on the damping effect of the shroud is reviewed by means of amplitude-frequency response and energy through the Newmark-β numerical method. The results demonstrate that the damping effect of the shroud by contact is more obvious than by friction and the amplitude-frequency curve of the shrouded blade shows a strong hard nonlinear phenomenon.

1. Introduction

As an important component of aero-engines, blades are subjected to high-cycle fatigue. In order to make the rotating blade more reliable, the method of adding shrouds to the blade is often used to solve the problem in engineering. The shroud can increase the rigidity and the natural frequency of the blade, and when the blade is vibrating, the working surface of the shroud can rub against each other to absorb vibration energy [1]. The process of contact vibration with shrouded blades is very complex and usually includes separation-contact-stick-slip states, with typical nonlinear characteristics.

Due to the complexity of nonlinear problems, it is difficult to obtain accurate dynamic responses. Therefore, many researchers use the "macroslip" model to study the motion of the contact surface of the shroud. This method regards the contact surface as a rigid body; when sliding, all the points on the contact surface are in the same state, and the contact can be approximated as point-to-point [2–4]. Menq and Yang [5] suggested that the friction interface is an elastic body if the normal load acting on the interface is high enough, and it is capable of modeling partial slip before all points slip. So, they investigated a two-dimensional model by assuming points of contact move in a circular path and dividing the contact into the parallel connection of some small macroslip model elements. In addition, the lumped mass model can be used to analyze the damping mechanism of the shrouded blade easily. At early stages, Menq et al. [6] analyzed the nonlinear friction of the contact surface by establishing a lumped mass model of a bladed disk with the shroud. Muszynska and Jones [7] simplified the shrouded blade into a lumped mass of multi-degree-of-freedom model and studied the dynamic response of the two-degree-of-freedom model as well as the four-degree-of-freedom model. Recently, Nan and Ren [8] modeled the shrouded blade as a mass-spring model and considered couplings of axial and tangential displacement of the shrouded blade. He et al. [9]

established a lumped mass model of integrally shrouded group blades considering centrifugal stiffening of the blade as well as rubbing and impact between adjacent shrouds. Machado et al. [10] compared and analyzed the most common compliant contact force models of the last decades, and results in terms of the dynamic simulations of multibody systems are presented, which allow the comparison of the similarities and differences among the models considered.

As technology progressed, researchers began to use continuum models to study the shrouded blades. At first, Bab et al. [11] studied the effects of flexible blades and rigid blades on the system, and they found the system with rigid blades becomes completely stable in higher values of the mass eccentricity compared to the system with flexible blades. Choi and Chou [12] modeled a shrouded blade as a pretwisted Timoshenko beam with varying cross section and used the modified differential quadrature method to analyze the vibration of elastically supported blades. However, they only considered the effect of the shroud's mass and did not study the effect of the contact surface. Szwedowicz et al. [13] studied the free and forced vibration of shrouded blade-disk systems through the analytical method and validated the analytical model by experiment, but they only considered the frictional effects. Cao et al. [14] proposed an approximate approach to study the dynamic responses of blades constrained by friction interfaces and investigated the nonlinear dynamic characteristics of blades. Cao et al. [15] investigated a full-circle stage of steam turbine with shroud and labyrinth seals under the steam exciting force by numerical simulator CFX. Chu et al. [16] used the average method to establish a nonlinear equation of motion and used blade's bending stiffness as the shroud's collision stiffness to study the rubbing response of the shrouded blade. Based on previous research [8], Nan [17] developed a model composed of springs and a cantilever beam carrying a mass to simulate the shrouded blade, considering the effects of the centrifugal stiffening, spin softening, and Coriolis force. Ma et al. [18] established a dynamic model of rotating shrouded blades and analyzed the effects of symmetric and asymmetric shroud gaps, rotational speeds, and aerodynamic force amplitudes on the dynamic characteristics of shrouded blades. Based on their previous work, Xie et al. [19] used two different impact models to analyze the effects of different parameters on the vibration responses of the shrouded blades. In previous studies, the blades were considered as beam model, but Ghazavi et al. [20] considered the blades as inverted pendulums, and the effect of rotor and blade damping as well as rotating speed is investigated.

In addition, some researchers used the finite element (FE) model to study the shrouded blade. Petrov [21] used the finite element method to analyze the influence of parameters such as the friction coefficient, contact surface stiffness (normal and tangential coefficients), clearances, interferences, and the normal stresses at the contact interfaces on the vibration response of the blade. Gu et al. [22–24] proposed a three-dimensional numerical friction contact model to investigate the nonlinear vibration of a damped blade through the FE model. Zucca et al. [25] computed the actual contact area on the shroud surface and the distribution of normal static loads through the FE model. Liu et al. [26, 27] proposed an improved hybrid frequency-time domain method to efficiently study the nonlinear response of blade systems subject to dry friction damping and established a shrouded blade model with frictional contact by the finite element method. Through different contact surfaces and different loading methods, the friction force was determined and the contact state between the contact surfaces of the shroud was analyzed.

In previous studies, researchers have constantly been improving the contact model of the shroud and used a variety of methods to solve the response of the blade, but few scholars analyzed the damping mechanism of the shroud comparing the damping effect of friction and contact and consider the influences of the shroud mass, and the contact force generated by the shroud during the contact process is not always linear. Based on Hunt KH's [28] nonlinear contact theory and considering the influences of the shroud mass, this paper established a contact force model with dry friction model to simulate the contact state of rotating shrouded blades. Then, taking the rotational speed, contact angle, friction coefficient, clearance, and shroud position as parameters, the vibration mechanism of the rotating shrouded blade is investigated from the perspective of nonlinear response and energy.

2. Dynamic Model and Equation

When the number of shroud blades on the disk is more than 6, the whole group of integrally shrouded blades will form a circular structure. In order to study the influence of contact force and friction force to the vibration characteristics of shrouded blades, it is reasonable to establish a model with three shroud blades, and the model diagram of shrouded blades is shown in Figure 1(a), and considering the mass of shroud and the rotational effects of the shrouded blade, a schematic of shrouded blades and the corresponding coordinate system is shown in Figure 1(b). The cantilever Euler–Bernoulli beam is used to simulate the flexible shrouded blade clamped on the rigid disk. Since the contact force and friction force in the proposed model are characterized by the relative motion, to simplify calculations, the blades on the right and left side will be assumed as fixed ground.

In Figure 1(b), $OXYZ$ is the global coordinate; $oxyz$ is the local coordinate of an arbitrary point Q on the blade; and R_d, ΩL, δ, m_s and $\widetilde{L}$ represent disk radius, rotational speed (rad/s), the length of blade, the clearance between adjacent shrouds, shroud mass, and the position of the shroud, respectively. It is worth noting that the x, y, and z directions are in accordance with the radial, flexural, and

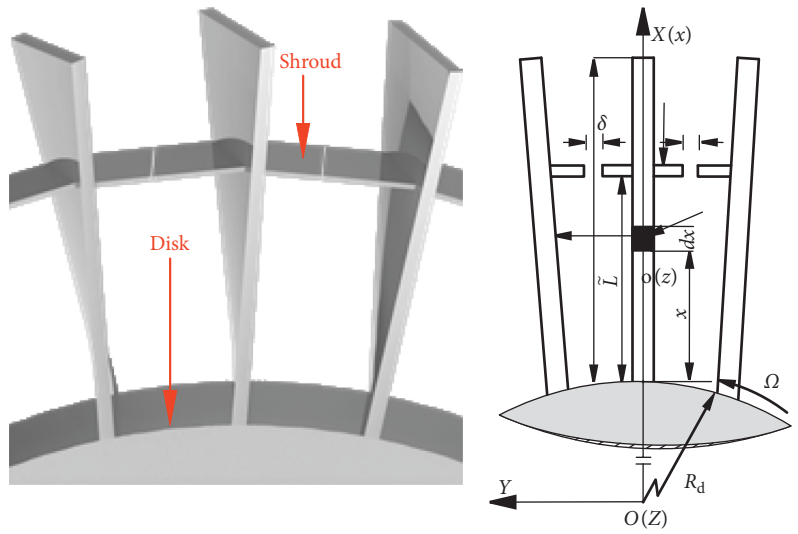

(a) (b)

Figure 1: (a) The model diagram of shrouded blades. (b) Schematic diagram of rotating shrouded blades in a constant speed.

swing directions of the rotating blade. In order to solve the kinetic energy of the blade, the displacement vectors $\mathbf{r}_Q$ of an arbitrary point Q in the global coordinate system can be expressed as

$$\mathbf{r}_Q = \mathbf{A}_1\left(\mathbf{r}_{Q0} + \boldsymbol{\delta}_Q\right) = \mathbf{A}_1\begin{bmatrix} R_d + x + u \\ v \\ w \end{bmatrix},$$

$$\mathbf{r}_{Q0} = \begin{bmatrix} R_d + x \\ 0 \\ 0 \end{bmatrix}, \tag{1}$$

$$\boldsymbol{\delta}_Q = \begin{bmatrix} u \\ v \\ w \end{bmatrix},$$

$$\mathbf{A}_1 = \begin{bmatrix} \cos\vartheta & \sin\vartheta & 0 \\ -\sin\vartheta & \cos\vartheta & 0 \\ 0 & 0 & 1 \end{bmatrix}, \tag{2}$$

where x is the position of the Q point on the x-axis of the local coordinate system and u, v, and w are the displacements of the Q point along the x, y, and z axes of the local coordinate system, respectively. $\mathbf{A}_1$ is the transformation matrix of the local coordinate system to the global coordinate system, $\vartheta = \Omega t$.

It is worth noting that because this paper considers the influence of the shroud mass, it is also necessary to solve the kinetic energy of the shroud, and the displacement vectors $\mathbf{r}_s$ of shroud in the global coordinate system can be expressed as

$$\mathbf{r}_s = \mathbf{A}_1\left(\mathbf{r}_{s0} + \boldsymbol{\delta}_s\right) = \mathbf{A}_1\begin{bmatrix} R_d + \tilde{L} + u_{\tilde{L}} \\ v_{\tilde{L}} \\ w_{\tilde{L}} \end{bmatrix},$$

$$\mathbf{r}_{s0} = \begin{bmatrix} R_d + \tilde{L} \\ 0 \\ 0 \end{bmatrix}, \tag{3}$$

$$\boldsymbol{\delta}_s = \begin{bmatrix} u_{\tilde{L}} \\ v_{\tilde{L}} \\ w_{\tilde{L}} \end{bmatrix},$$

where $\tilde{L}$ is the position of the shroud on blade. In this paper, $\tilde{L} = 2L/3$; $u_{\tilde{L}}$, $v_{\tilde{L}}$, and $w_{\tilde{L}}$ are the displacements of the shroud along the x, y, and z axes of the local coordinate system, respectively.

The velocity vector $\mathbf{v}_Q$ of point Q and the velocity vector $\mathbf{v}_s$ of the shroud can be written as

$$\begin{cases} \mathbf{v}_Q = \dot{\mathbf{r}}_Q, \\ \mathbf{v}_s = \dot{\mathbf{r}}_s. \end{cases} \tag{4}$$

So, the total kinetic energy T of the shrouded blade can be written as

$$\begin{cases} T = T_b + T_s, \\ T_b = \dfrac{1}{2}\displaystyle\int_0^L \Delta m \mathbf{v}_Q^2 dx = \frac{1}{2}\rho A \int_0^L \dot{\mathbf{r}}_Q^2 dx, \\ T_s = \dfrac{1}{2} m_s \dot{\mathbf{r}}_s^2, \end{cases} \tag{5}$$

where ρ denotes the density of blade and A is the cross-sectional area of the blade.

Substituting formulas (1)~(4) into formula (5),

$$\begin{aligned} T_{\mathrm{b}} = {} & \frac{1}{2}\int_0^L \Big[\dot{u}^2 + \dot{v}^2 + \dot{w}^2 + 2\Omega v\dot{u} - 2\Omega u\dot{v} - 2\Omega\left(R_{\mathrm{d}} + x\right)\dot{v} \\ & + \Omega^2\left(R_{\mathrm{d}} + x\right)^2 + 2\Omega^2\left(R_{\mathrm{d}} + x\right)u + \Omega^2\left(u^2 + v^2\right)\Big]\rho A dx, \\ T_{\mathrm{s}} = {} & \frac{1}{2}m_{\mathrm{s}}\Big[\dot{u}_{\widetilde{L}}^2 + \dot{v}_{\widetilde{L}}^2 + \dot{w}_{\widetilde{L}}^2 + 2\Omega v_{\widetilde{L}}\dot{u}_{\widetilde{L}} - 2\Omega u_{\widetilde{L}}\dot{v}_{\widetilde{L}} \\ & - 2\Omega\left(R_{\mathrm{d}} + x + \widetilde{L}\right)\dot{v}_{\widetilde{L}} + \Omega^2\left(R_{\mathrm{d}} + x + \widetilde{L}\right)^2 \\ & + 2\Omega^2\left(R_{\mathrm{d}} + x + \widetilde{L}\right)u_{\widetilde{L}} + \Omega^2\left(u_{\widetilde{L}}^2 + v_{\widetilde{L}}^2\right)\Big]. \end{aligned} \tag{6}$$

The effect of the shroud on the structural stiffness of the blade is ignored, so the total potential energy U of the blade is given as

$$\begin{aligned} U = {} & \frac{1}{2}\int_0^L EA\left(\frac{\partial u}{\partial x}\right)^2 dx + \frac{1}{2}\left[\int_0^L EI_z\left(\frac{\partial^2 v}{\partial x^2}\right)^2 dx\right. \\ & \left. + \int_0^L f_{\mathrm{c}}\left(\frac{\partial v}{\partial x}\right)^2 dx\right] + \frac{1}{2}\left[\int_0^L EI_y\left(\frac{\partial^2 w}{\partial x^2}\right)^2 dx\right. \\ & \left. + \int_0^L f_{\mathrm{c}}\left(\frac{\partial w}{\partial x}\right)^2 dx\right], \end{aligned} \tag{7}$$

where E is the modulus of elasticity, I_{z} is the cross section inertia moment of z direction of blade, I_{y} is the cross section inertia moment of y direction of blade, and $f_{\mathrm{c}}(x)$ is the centrifugal force and the expression is

$$f_{\mathrm{c}}(x) = \begin{cases} \rho A\Omega^2\displaystyle\int_x^L \left(R_{\mathrm{d}} + x\right)dx + m_{\mathrm{s}}\Omega^2\left(R_{\mathrm{d}} + \widetilde{L}\right), & 0 \le x \le \widetilde{L}, \\ \rho A\Omega^2\displaystyle\int_x^L \left(R_{\mathrm{d}} + x\right)dx, & \widetilde{L} < x \le L. \end{cases} \tag{8}$$

By using the Galerkin method to discretize the radial, flexural, and swing displacements of blade with their first n modes and introducing the generalized coordinates $q_{ui}(t)$, $q_{vi}(t)$, and $q_{wi}(t)$, according to the assumed mode method, the radial displacement $u(x, t)$, flexural displacement $v(x, t)$, and swing displacement $w(x, t)$ of the blade can be transformed into

$$\begin{cases} u(x,t) = \displaystyle\sum_{i=1}^{n} \varphi_i(x) q_{ui}(t) = \boldsymbol{\varphi}^T \mathbf{q}_u, \\ v(x,t) = \displaystyle\sum_{i=1}^{n} \phi_i(x) q_{vi}(t) = \boldsymbol{\phi}^T \mathbf{q}_v, \\ w(x,t) = \displaystyle\sum_{i=1}^{n} \eta_i(x) q_{wi}(t) = \boldsymbol{\eta}^T \mathbf{q}_w, \end{cases} \tag{9}$$

where $\varphi_i(x)$, $\phi_i(x)$, and $\eta_i(x)$ are the ith mode shape functions for radial, flexural, and swing vibrations, respectively, whose expressions can be written as follows [18]:

$$\begin{cases} \varphi_i(x) = \sin\left(\dfrac{2i-1}{2}\dfrac{\pi x}{L}\right), \\ \phi_i(x) = \mathrm{ch}\dfrac{\lambda_i}{L}x - \cos\dfrac{\lambda_i}{L}x - \dfrac{\mathrm{sh}\lambda_i - \sin\lambda_i}{\mathrm{ch}\lambda_i + \cos\lambda_i}\left(\mathrm{sh}\dfrac{\lambda_i}{L}x - \sin\dfrac{\lambda_i}{L}x\right), \\ \eta_i(x) = \mathrm{ch}\dfrac{\lambda_i}{L}x - \cos\dfrac{\lambda_i}{L}x - \dfrac{\mathrm{sh}\lambda_i - \sin\lambda_i}{\mathrm{ch}\lambda_i + \cos\lambda_i}\left(\mathrm{sh}\dfrac{\lambda_i}{L}x - \sin\dfrac{\lambda_i}{L}x\right), \end{cases} \tag{10}$$

where $i = 1, 2, 3, \ldots, n$ (n is the number of modal truncation), and in this paper, $n = 3$. λ_i is the eigenvalue of the ith mode shape function in flexural and swing direction, which can be obtained by the frequency equation [18]:

$$1 + \cos\lambda_i \mathrm{ch}\lambda_i = 0. \tag{11}$$

Substituting the discrete displacement of the blade into the kinetic energy and potential energy equation, by using the Lagrange equation, the equations of motion of the shrouded blade can be written as

$$\mathbf{M}\ddot{\mathbf{X}} + (\mathbf{C} + \mathbf{G})\dot{\mathbf{X}} + \left(\mathbf{K}_{\mathrm{b}} + \mathbf{K}_{\mathrm{c}} + \mathbf{K}_{\mathrm{s}}\right)\mathbf{X} = \mathbf{F}, \tag{12}$$

where $\mathbf{X}$ is the generalized coordinates vector and $\mathbf{M}$, $\mathbf{G}$, $\mathbf{C}$, $\mathbf{K}_{\mathrm{b}}$, $\mathbf{K}_{\mathrm{c}}$, and $\mathbf{K}_{\mathrm{s}}$ are the mass matrix, Coriolis force matrix, damping matrix, structural stiffness matrix, centrifugal stiffening matrix, and spin softening matrix, respectively. $\mathbf{F}$ is the external force vector that contains external excitation, contact force, and friction force; the expressions of contact force and friction force will be derived in the next section; the sinusoidal excitation ($F_0 \sin \omega t$) is used as the external excitation and is applied in the flexural and swing directions of the blade. Because the damping coefficient is mainly obtained by the test, this paper uses the Rayleigh damping model to describe the damping of the blade, and the expression can be written as

$$\mathbf{C} = \alpha_0\mathbf{M} + \beta_0\mathbf{K}_{\mathrm{b}}, \tag{13}$$

where $\alpha_0 = 4\pi((\xi_2/\omega_2) - (\xi_1/\omega_1))/((1/\omega_2^2) - (1/\omega_1^2))$; $\beta_0 = (1/\pi)(\xi_2\omega_2 - \xi_1\omega_1)/(\omega_2^2 - \omega_1^2)$; ω_1 and ω_2 are first- and second-order circular frequency, respectively; ξ_1 and ξ_2 are the first- and second-order damping coefficient, respectively; all the above expressions of these matrices are shown in Appendix.

3. Contact Model

Figure 2 is a specific model diagram of the shroud blade, in which the shroud is equivalent to a spring k_{h}, and the blade located in the middle bears the contact force and friction from the left or right-side shroud when vibrating, where α is the contact angle of the shroud, δ is the clearance between the adjacent shrouds, k_{t} is the shear stiffness of friction

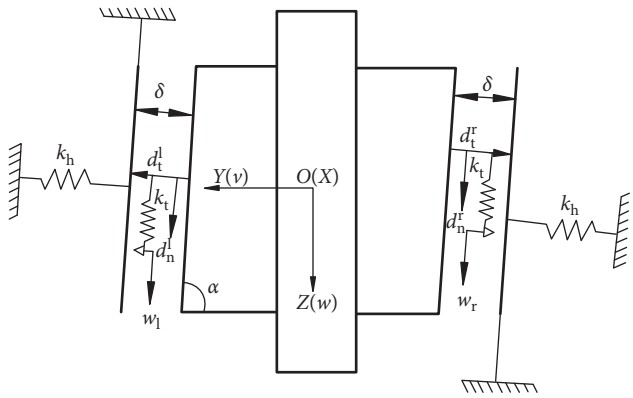

Figure 2: A specific model diagram of shrouded blades.

model, d_t^l and d_t^r are the tangential displacement of the left and right-side shroud, respectively, and d_n^l and d_n^r are the normal displacement of the left and right-side shroud.

Based on the contact theory proposed by Hunt and Crossley [28], the normal pressure on the total contact surface F_N can be expressed as

$$F_N = F_N^l + F_N^r, \tag{14}$$

$$F_N^l = \begin{cases} -k_h\left(d_n^r - \delta\right)^{3/2}, & \delta < d_n^r, \\ 0, & d_n^l \le \delta, \end{cases}$$
$$F_N^r = \begin{cases} k_h\left(\left|d_n^l\right| - \delta\right)^{3/2}, & d_n^l < -\delta, \\ 0, & -\delta \le d_n^l, \end{cases} \tag{15}$$

where F_N^l represents the contact force when the middle blade is in contact with the left-side shroud and F_N^r represents the contact force when the middle blade is in contact with the right-side shroud, since it is assumed that the blades on both sides are fixed; so, according to the geometric relationship,

$$\begin{cases} d_n^l = d_n^r = v_{\tilde{L}}\sin\ \alpha - w_{\tilde{L}}\cos\ \alpha, \\ d_t^l = d_t^r = v_{\tilde{L}}\cos\ \alpha + w_{\tilde{L}}\sin\ \alpha. \end{cases} \tag{16}$$

The friction model is considered as a macroscopic slip model with the variable normal load, and the total friction force F_f can be expressed as

$$F_f = F_f^l + F_f^r,$$
$$F_f^l = \begin{cases} k_t\left(d_t^l - w_l\right), & k_t\left|d_t^l - w_l\right| < \mu F_N^l, \\ \mu F_{Nl}\,\mathrm{sgn}\left(\dot{w}l\right), & k_t\left|d_t^l - w_l\right| \ge \mu F_N^l, \end{cases}$$
$$F_f^r = \begin{cases} k_t\left(d_t^r - w_r\right), & k_t\left|d_t^r - w_r\right| < \mu F_N^r, \\ \mu F_{Nr}\,\mathrm{sgn}\left(\dot{w}_r\right), & k_t\left|d_t^r - w_r\right| \ge \mu F_N^r, \end{cases} \tag{17}$$

where F_f^l denotes the friction force when the middle blade is in contact with the left-side shroud and F_f^r denotes the friction force when the middle blade is in contact with the right-side shroud. w_r and $\dot{w}_r$ are the displacement and velocity of frictional damper of the right-side contact surface, respectively. w_l and $\dot{w}_l$ are the displacement and velocity of frictional damper of the left-side contact surface, respectively.

Taking the left-side contact surface as an example, when the elastic force $k_t|d_t^l - w_l|$ generated by the shear spring on the contact surface is less than the sliding friction force μF_N^l, the contact surface will be in a stick state, and thus the velocity of the frictional damper $\dot{w}_r = 0$; when the elastic force generated $k_t|d_t^l - w_l|$ is greater than the sliding friction force μF_N^l, the contact surface will be in a slip state, so the velocity of the frictional damper $\dot{w}_r = \dot{d}_t^l$; then, we can obtain

$$\dot{w}_l = \begin{cases} 0, & \text{stick}, \\ \dot{d}_t^l, & \text{slip}. \end{cases} \tag{18}$$

The value of w_l can be obtained in the iterative calculation process:

$$w_{lq} = \begin{cases} w_{l\,(q-1)}, & \text{stick}, \\ w_{l\,(q-1)} + \dot{d}_{t\,(q-1)}^l \times \Delta t, & \text{slip}, \end{cases} \tag{19}$$

where q represents the order of the iterations and $\dot{d}_t^l$ represents the velocity of the left-side contact surface.

$$\dot{d}_t^l = \dot{v}_{\tilde{L}}\sin\ \alpha - \dot{w}_{\tilde{L}}\cos\ \alpha. \tag{20}$$

4. Numerical Examples and Discussion

The vibration characteristics of the shrouded blade are closely related to the rotational speed and the structural parameters of the shroud, such as contact angle, friction coefficient, clearance, and shroud position. Alterations in these structural parameters affect the response characteristics of the blade and then affect the damping effect of the shroud. Therefore, by analyzing the influence of these structural parameters on the response characteristics of the blade, the damping mechanism of the shroud can be deeply understood.

The parameters of the rotating shrouded blade are given in Table 1.

The analytical model of the shroud blade is verified by comparing the natural frequencies with the corresponding finite element model. The Beam188 element and the Mass21 element are used to simulate the model of the shrouded blade with concentrated mass at a distance of 2/3 from the root. And the first three orders of bending frequencies f_{n1}, f_{n2}, and f_{n3} are shown in Figure 3, which shows that the results of the analytical model are very consistent with the results of the finite element model, with only a largest error about 4.55% for the second natural frequency.

4.1. Rotational Speeds. Taking the GE90 engine as an example, its working speed is 10396 r/min. Therefore, the speed of 1000 rad/s is selected as the study parameter, and considering the starting and stopping process of the engine, 500 rad/s and 800 rad/s are also selected as the study parameters. In order to investigate the effect of rotational speed on the response characteristics of the blade, the amplitude-frequency curves at different rotational speeds of the

Table 1: The parameters of the rotating shrouded blade.

No.	Physical quantity (symbol)	Value/unit
1	Disk radius (R_d)	350 mm
2	Blade length (L)	150 mm
3	Blade width (b)	60 mm
4	Blade thickness (h)	7 mm
5	Shroud mass (m_s)	0.04396 kg
6	Shroud position ($\widetilde{L}$)	$2/3 \times L$
7	Young's modulus (E)	200 GPa
8	Poisson's ratio (ν)	0.3
9	Density (ρ)	7850 kg/m^3
10	Clearance (δ)	0.1 mm
11	Friction shear stiffness (k_t)	1×10^7 N/m
12	Contact stiffness (k_h)	1×10^7 N/m
13	Contact angle (α)	$\pi/4$
14	The coefficient of friction (μ)	0.2
15	Excitation amplitude (F_0)	350 N

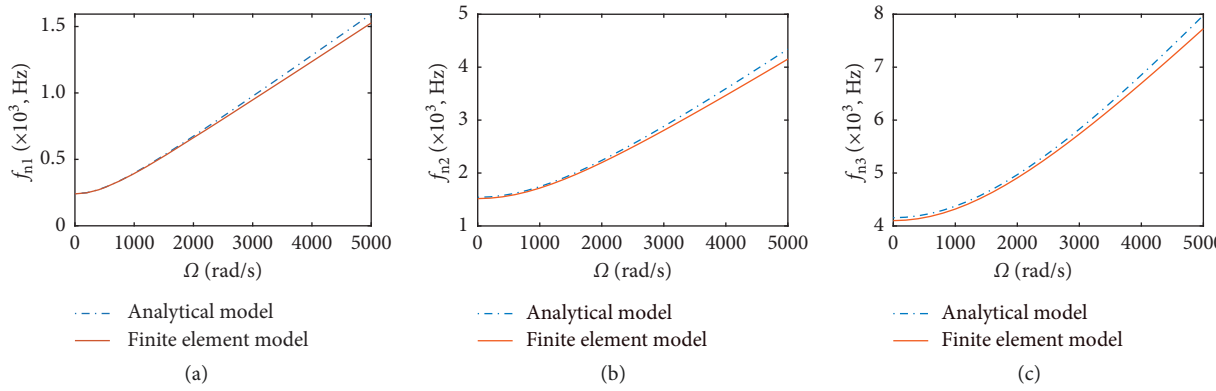

Figure 3: Dynamic frequencies obtained from FE model and analytical model.

shrouded blade's tip as well as the nonshrouded blade's tip are depicted in Figure 4. One can observe from Figure 3 that the resonance frequency increases with the increase of rotational speed, but the resonance peak decreases with the increase of rotational speed. Especially, the resonance peak of the shrouded blade is much lower than that of the nonshrouded blade, and the resonance frequency of a shrouded blade is larger than the nonshrouded blades. In addition, the amplitude-frequency curves of the shrouded blade show a strong hard nonlinearity; it is because the existence of shroud is equivalent to increasing the constraint stiffness of the blade, so the natural frequency of the blade will increase, and the contact force and friction generated by shroud are nonlinear, resulting in a hard nonlinear phenomenon. And due to the existence of hard nonlinearity, the vibration amplitude of the blade is reduced, so the stability of the blade response is increased, which indicates that the shroud brings an obvious damping effect.

For the sake of further studying the influence of rotational speed, it is necessary to analyze the contact force and the friction force on the shroud's contact surface at different rotational speeds. To make the phenomenon more obvious, the resonant frequency corresponding to the highest point of each curve in Figure 4 is selected as the external excitation

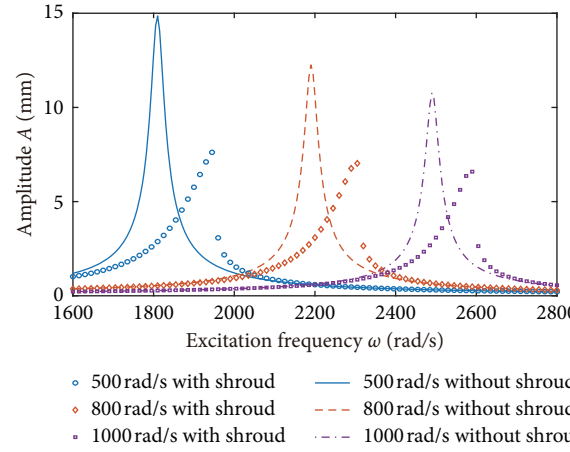

Figure 4: The amplitude-frequency curves at different rotational speeds.

frequency. Figures 5(a) and 5(b) show the variations in contact force and friction force at different rotational speeds, respectively. d_n (contains d_n^l and d_n^r) represents the displacement of the shrouded blade along the normal direction of the shroud's contact surface; d_t (contains d_t^l and d_t^r)

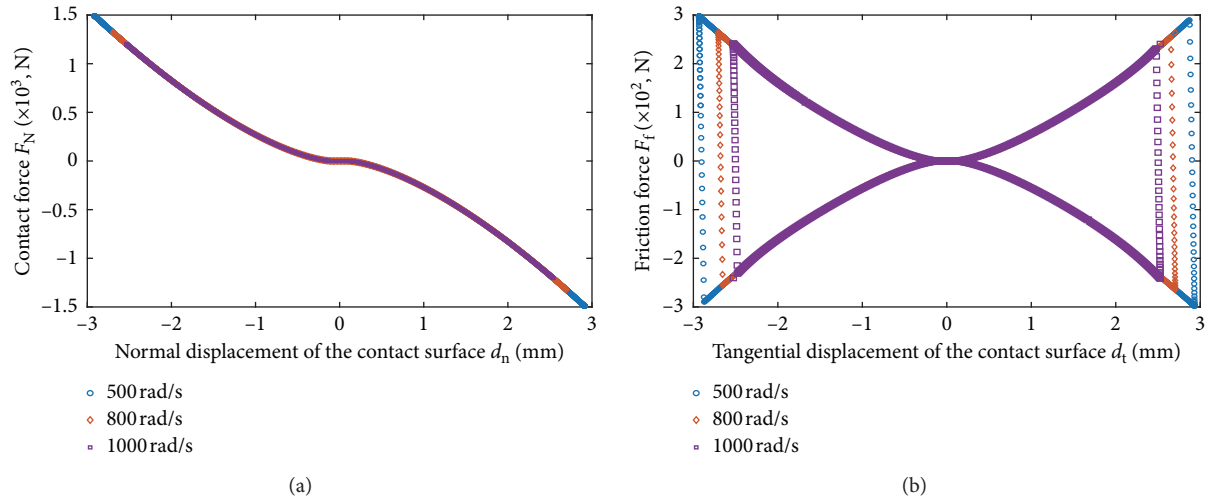

Figure 5: The curves of force at different speeds. (a) Contact forces. (b) Friction forces.

represents the displacement of the shrouded blade along the tangential direction of the shroud's contact surface. It can be observed from the Figures 5(a) and 5(b) that with the increase of the rotational speed, the maximum value of the contact force and the friction force all show the same trend, and the maximum value of both decreases as the rotational speed increases.

When the shroud contacts with the adjacent shroud, a portion of the shrouded blade's energy is stored due to the shroud's elastic deformation as the shroud is equivalent to a spring k_h in this paper, and the corresponding expression in a single motion cycle of the rotating shrouded blade is as equation (21). Meanwhile, a portion of the shrouded blade's energy is dissipated due to the friction of the contact surface. Therefore, from the perspective of energy, we can investigate the damping situation of the shroud more deeply and can compare the damping effect of the contact and the friction. The root mean square value of the maximum energy of the rotating shrouded blade in a single motion cycle is selected as the total energy. By comparing the ratio of the elastic potential energy by the contact force and the consumed energy by the friction force to the total energy of the shrouded blade in one single motion cycle, we can study the damping contributions provided by contact and friction forces during blade vibration.

$$E_F = \sum\left[F_{Nq}^{l}\left(d_{nq}^{r} - \delta\right) + F_{Nq}^{r}\left(\left|d_{nq}^{l}\right| - \delta\right)\right], \tag{21}$$

where q represents the order of the iterations, in a single motion cycle.

Figure 6(a) is the ratio of elastic potential energy stored by the contact force in one motion period of the shrouded blade at different speeds and Figure 6(b) is the ratio of energy dissipated by the friction force in one motion period of the shrouded blade at different speeds. It can be observed from Figures 6(a) and 6(b) that with the increase of the rotational speed, the maximum value of the energy storage ratio and the maximum value of the energy dissipation ratio all show the same trend as Figures 5(a) and 5(b). It is also noteworthy that the ratio of energy dissipated by the friction force is lower than the ratio of energy stored by the contact force, which can be demonstrated that during the vibration damping process of the shroud, the contact force plays a more significant role than the friction force.

4.2. Contact Angles. For the sake of studying the effect of the contact angle on the damping effect of the shroud, the amplitude-frequency curves of the shrouded blade's tip at different contact angles are shown in Figure 7, with the rotational speed of 1000 rad/s. It can be observed from Figure 7 that the resonance frequency keeps increasing as the contact angle increases. However, the resonance peak shows a different trend; the resonance peak decreases with the contact angle varying from 30° to 45°, but when the contact angle varies from 45° to 90°, the resonance peak starts to increase. Therefore, when the contact angle is 30°, the shroud has the worst damping effect, and when the contact angle is 45°, the shroud has the best suppression effect on the resonance peak of the blade; when the contact angle is 90°, the shroud has the greatest increase in the frequency. It is worth noting that as the contact angle increases, the hard nonlinearity of the amplitude-frequency curve becomes obvious.

In order to study the influence of the contact angle on the damping effect of the shroud, the curves of the contact force and the friction force at the different contact angles can be drawn as shown in Figures 8(a)–8(c), with the rotational speed of 1000 rad/s and the resonant frequency corresponding to the highest point of each curve in Figure 7 selected as the external excitation frequency. It can be observed from Figure 8(a) that as the contact angle increases, the maximum value of the contact force increases continuously, but when the contact angle increases to 60°, the increase in the maximum value of the contact force starts to decrease. And in Figure 8(b), as the contact angle increases, the range of the friction force begins to narrow, but the maximum the friction force begins to increase. This is because the contact force generated by the contact surface of

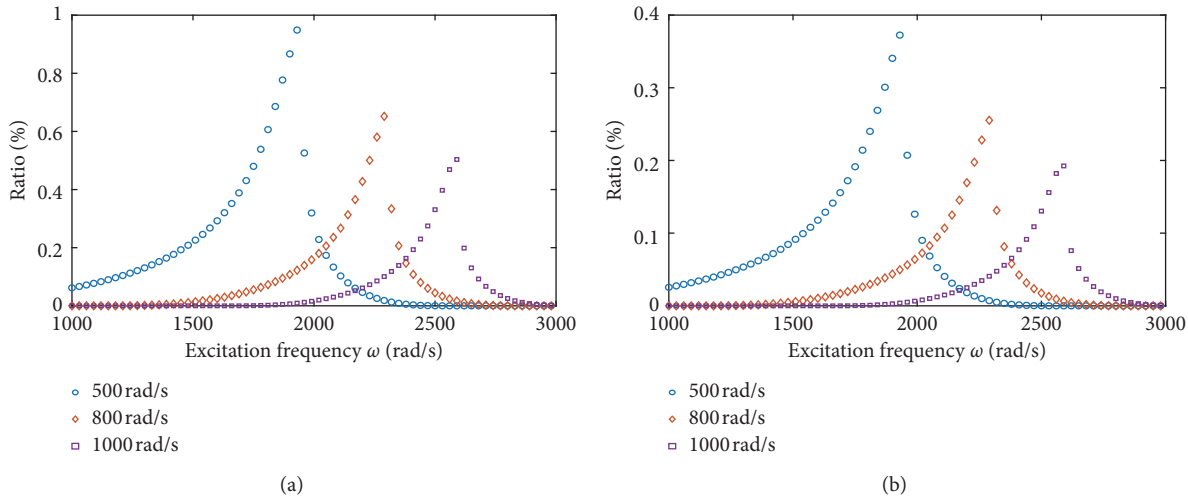

Figure 6: The energy ratio at different speeds. (a) Energy storage by contact force. (b) Energy consumption by friction force.

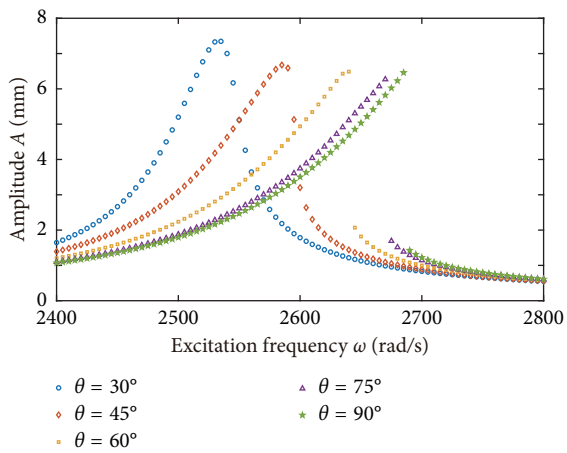

Figure 7: The amplitude-frequency curves at different contact angles.

the shroud is also greater when the contact angle is large; the friction force generated when the contact surface slips is also increased. Especially, in Figure 8(c), when the contact angle is 90°, the type of the friction force curve changes. This is because the displacement in the friction direction is only provided by the vibration displacement of the shrouded blade in the swing direction and the shroud blade's vibration in the swing direction is very weak and the friction force is small.

In order to investigate the effect of the contact angle on the damping effect of the shroud from the perspective of energy, the energy storage ratios of the contact force at different contact angles are shown in Figure 9(a), and the energy dissipation ratios of the friction force for different contact angles are shown in Figure 9(b) with the rotational speed of 1000 rad/s. The energy stored through contact increases with the contact angle rising from 30° to 90°. The energy dissipated through friction increases with the increase of the contact angle from 30° to 45°; however, after the contact angle reaches 45°, the energy dissipated through friction starts to decrease. When the contact angle is 90°, the energy dissipated through friction decreases to zero, thus resulting in a phenomenon in which the resonance amplitude becomes smaller at the contact angle of 45° in Figure 7.

4.3. Friction Coefficients. The amplitude-frequency curves of the shrouded blade's tip at different friction coefficients are shown in Figure 10, with the rotational speed of 1000 rad/s. As the friction coefficient varies from 0 to 0.5, the resonant peak of the blade decreases continuously, which means that the shroud structure has a better suppression effect on the resonant peak of the blade when the friction coefficient is larger. However, the resonance frequency of the blade hardly changes with the friction coefficient varying from 0 to 0.5. And as the friction coefficient increases, the hard nonlinear phenomenon of the amplitude-frequency curve becomes weak.

In order to further investigate the influence of the friction coefficient on the damping effect of the shroud, the curves of the contact force and the friction force at different friction coefficients are shown in Figures 11(a) and 11(b), with the rotational speed of 1000 rad/s and the resonant frequency corresponding to the highest point of each curve in Figure 10 selected as the external excitation frequency. As the friction coefficient varies from 0 to 0.5, the maximum value of the contact force decreases, but the maximum value of the friction force keeps increasing. Therefore, when the friction coefficient is larger, the contact surface can generate greater friction force to suppress the resonance amplitude of the blade.

For the sake of investigating the influence of the friction coefficient on the damping effect of the shroud from the perspective of energy, the energy storage ratios of the contact force at different friction coefficients are shown in Figure 12(a), and the energy dissipation ratios of the friction force at different friction coefficients are shown in Figure 12(b), with the rotational speed of 1000 rad/s. As the friction coefficient varies from 0 to 0.50, the energy stored

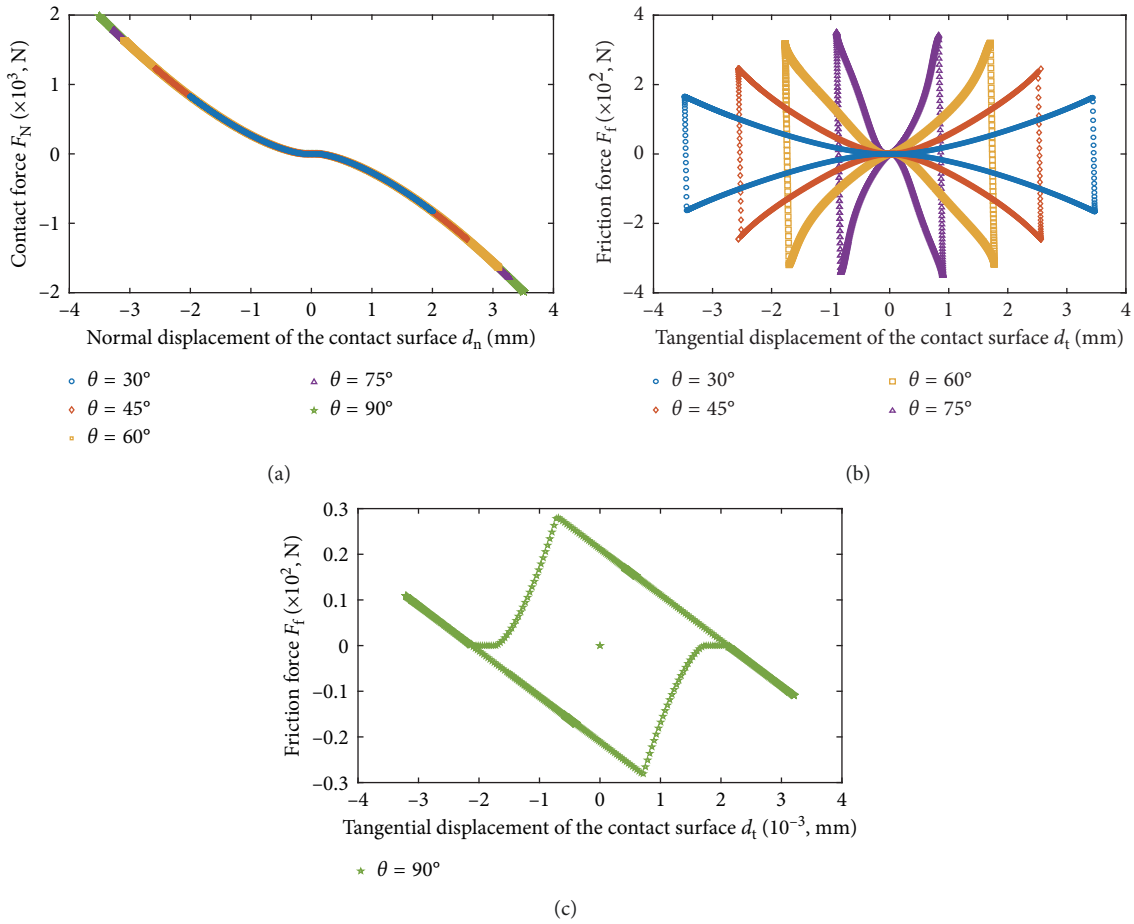

Figure 8: The curves of force at different angles. (a) Contact forces. (b) Friction forces (30°, 45°, 60°, and 75°). (c) Friction forces (90°).

through the contact force has decreased slightly, but the energy dissipated through the friction force increases continuously.

4.4. Clearances. The variation of clearance will affect the ease of shroud's contact and further affect the damping effect of the shroud. So, to study the effect of the clearance on the damping effect of the shroud, the amplitude-frequency curves of the shrouded blade's tip at different clearances are shown in Figure 13, with the rotational speed of 1000 rad/s. When the clearance rises from 0 mm to 2.0 mm, the resonant amplitude of the blade increases and the resonance frequency decreases. Especially, when the clearance rises to 2.0 mm, the resonance peak greatly increases. When the clearance reduces to 0 mm, the resonant amplitude decreases and the resonant frequency has a large improvement. Therefore, large clearance is not conducive to the damping effect of the shroud. It is worth noting that the hard nonlinear phenomenon of the amplitude-frequency curve of the shrouded blade becomes very obvious when the clearance is increased to 0.5 mm.

In order to further study the effect of the clearance on the damping effect of the shroud, the curves of the contact force and the friction force at different clearances can be drawn as shown in Figures 14(a) and 14(b), with the rotational speed of 1000 rad/s and the resonant frequency corresponding to the highest point of each curve in Figure 13 selected as the external excitation frequency. With the clearance increasing, the range of the null contact force is gradually widening, which indicates that the condition for contact between adjacent shrouds becomes more restrictive and requires more significant displacement of the shrouded blade. In addition, the maximum contact force and friction force greatly reduce with the increasing clearance.

For the purpose of investigating the effect of the clearance on the damping effect of the shroud from the perspective of energy, the energy storage ratios of the contact force at different clearances are shown in Figure 15(a) and the energy dissipation ratios of the friction force at different clearances are shown in Figure 15(b), with the rotational speed of 1000 rad/s. As the clearance increases, the energy stored by the contact force and the energy dissipated by the friction force are reduced in the resonance region. Especially, when the clearance reaches 2.0 mm, the shroud structure can only transfer energy by contact and friction in the resonance region when the shrouded blade vibrates.

4.5. Shroud Positions. Through the above analysis, it can be concluded that the damping effect of the shroud has a very important relationship with the contact force and the friction force generated on the contact surface and the energy

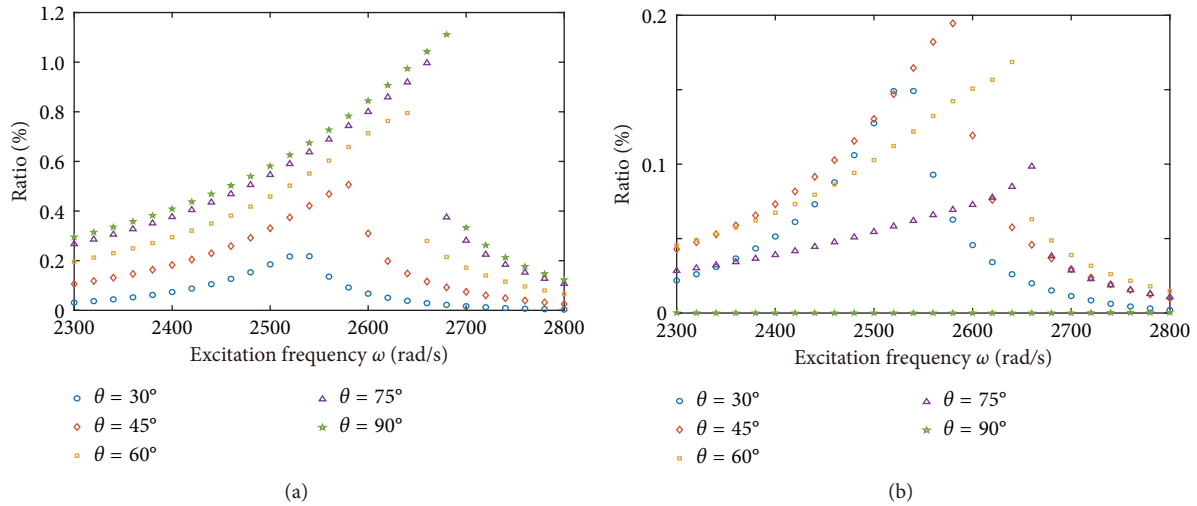

Figure 9: The energy ratio at different contact angles. (a) Energy storage by the contact force. (b) Energy consumption by the friction force.

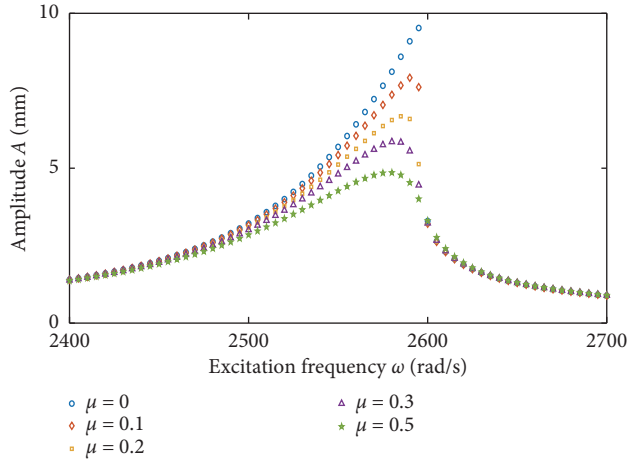

Figure 10: The amplitude-frequency curves at different friction coefficients.

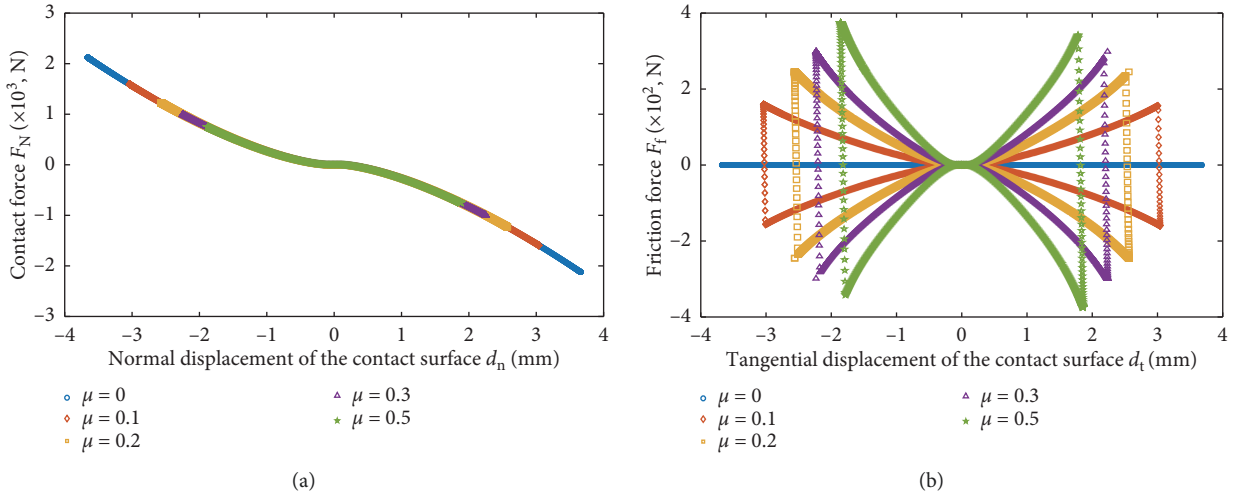

Figure 11: The curves of force at different friction coefficients. (a) Contact forces. (b) Friction forces.

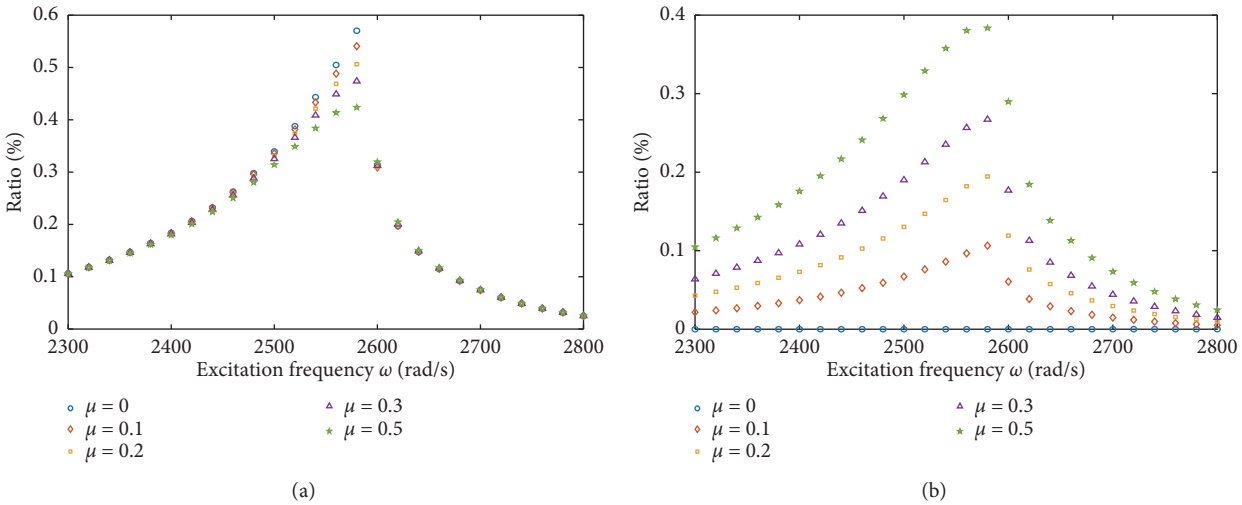

FIGURE 12: The energy ratio at different friction coefficients. (a) The ratio of energy storage by the contact force. (b) The ratio of energy consumption by the friction force.

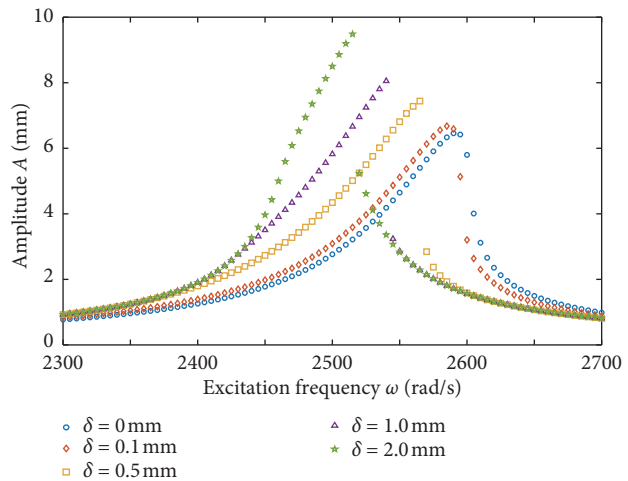

FIGURE 13: The amplitude-frequency curves at different clearances.

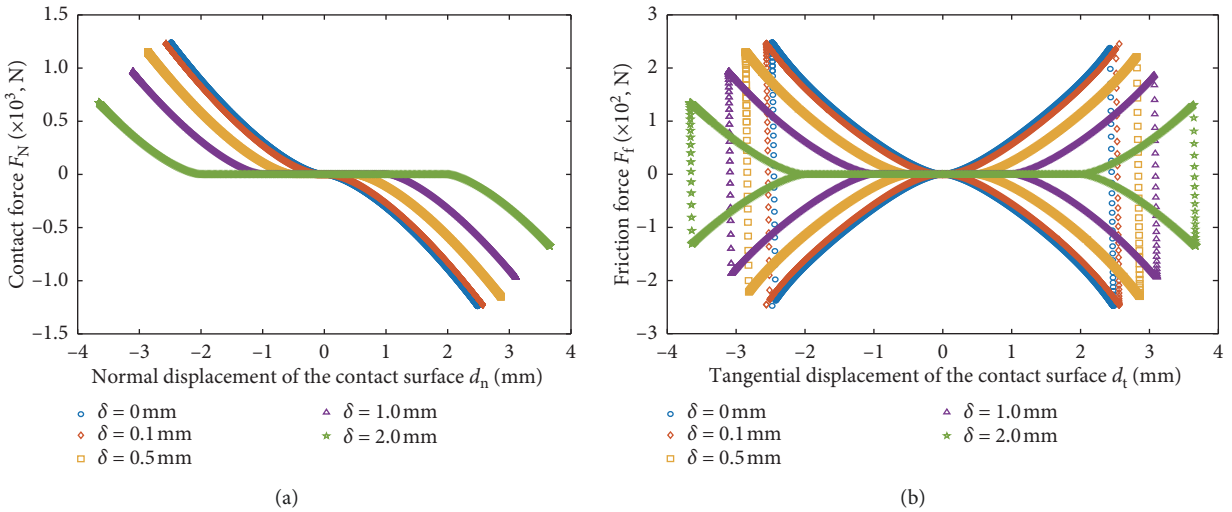

FIGURE 14: The curves of force at different clearances. (a) Contact forces. (b) Friction forces.

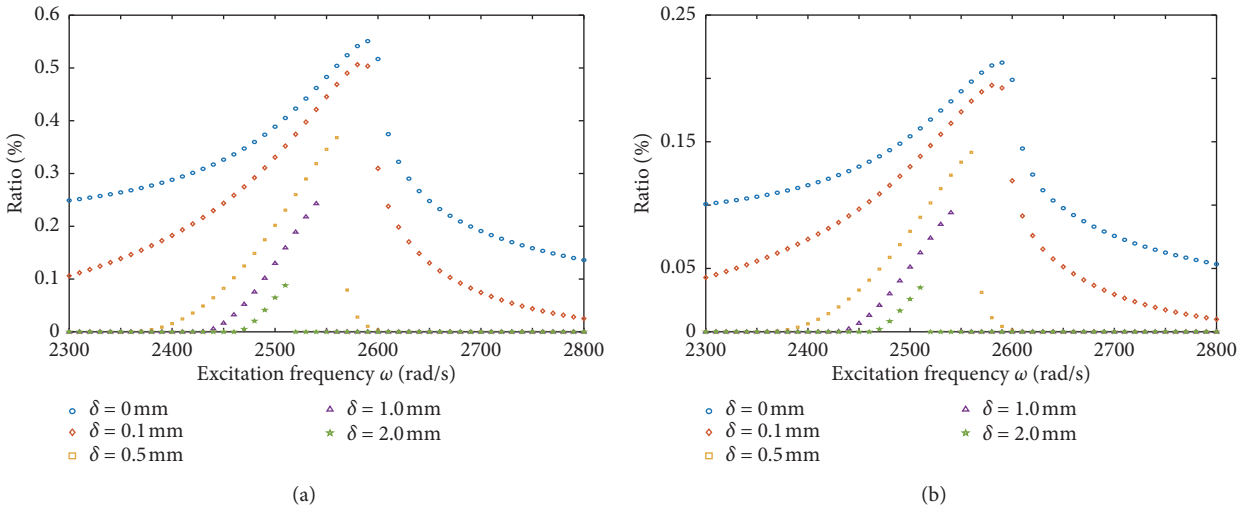

Figure 15: The energy ratio at different clearances. (a) The ratio of energy storage by the contact force. (b) The ratio of energy consumption by the friction force.

value transferred through contact and friction. According to equations (14) and (16), the contact force and the friction force generated by the contact surface have an important relationship with the relative displacement of the contact surface.

Therefore, for studying the effect of the different shroud positions on the damping effect of the shroud, the amplitude-frequency curves of the shrouded blade's tip at different shroud positions are depicted in Figure 16, with the rotational speed of 1000 rad/s. L is the length of the blade, $1/4 \times L$ indicates that the shroud position is near the root of the blade, and $1 \times L$ indicates that the shroud position is at the tip of the blade. It can be observed from Figure 16 that when the shroud position is near the blade root, the shroud structure has almost no damping effect, and the amplitude-frequency curve shows a linear variation. When the shroud position is rising to the middle of the blade, the damping effect of the shroud starts to become obvious, the resonance peak of the blade reduces, and the resonance frequency increases greatly, which indicates that the closer the shroud structure is to the tip of the blade, the better the damping effect is.

In order to further study the influence of the position on the damping effect of the shroud, the curves of the contact force and the friction force at different shroud positions are depicted in Figures 17(a) and 17(b), with the rotational speed of 1000 rad/s and the resonant frequency corresponding to the highest point of each curve in Figure 16 selected as the external excitation frequency. As the position rises, the maximum value of both the contact force and the friction force increases, but after the position rises to $2/3 \times L$, the maximum values of the contact force and the friction force start to decrease.

For the purpose of investigating the effect of position on the damping effect of the shroud from the perspective of energy, the energy storage ratios of the contact force at different shroud positions are depicted in Figure 18(a) and the energy consumption ratios of the friction force at

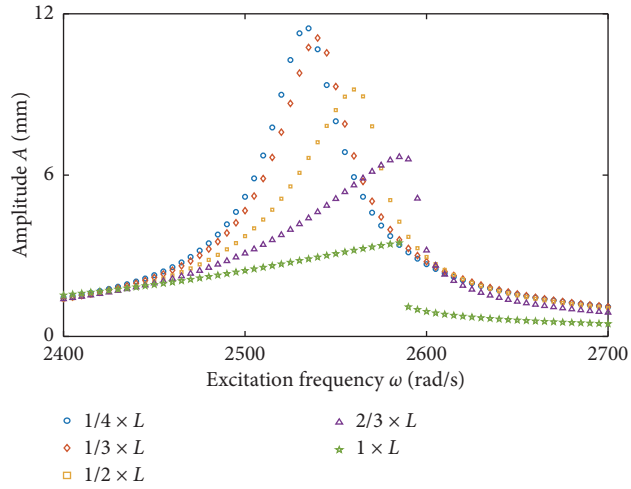

Figure 16: The amplitude-frequency curves at different shroud positions.

different shroud positions are depicted in Figure 18(b), with the rotational speed of 1000 rad/s. When the position is located at the root of the blade, the energy transferred by the contact force and the friction force is almost zero. And when the shroud is rising to the middle of the blade, the energy transferred by the contact force as well as the friction force becomes obvious. More importantly, when the shroud is located at the tip of the blade, the stored energy ratio approaches 1.4% and the energy dissipated through friction is only 0.6%. It is further explained that the damping effect of the shroud by contact is more obvious than by friction.

5. Conclusions

In this paper, the dynamic equation of the rotating shrouded blade considering the shroud mass is established, and the expression of dry friction and contact forces is derived. The

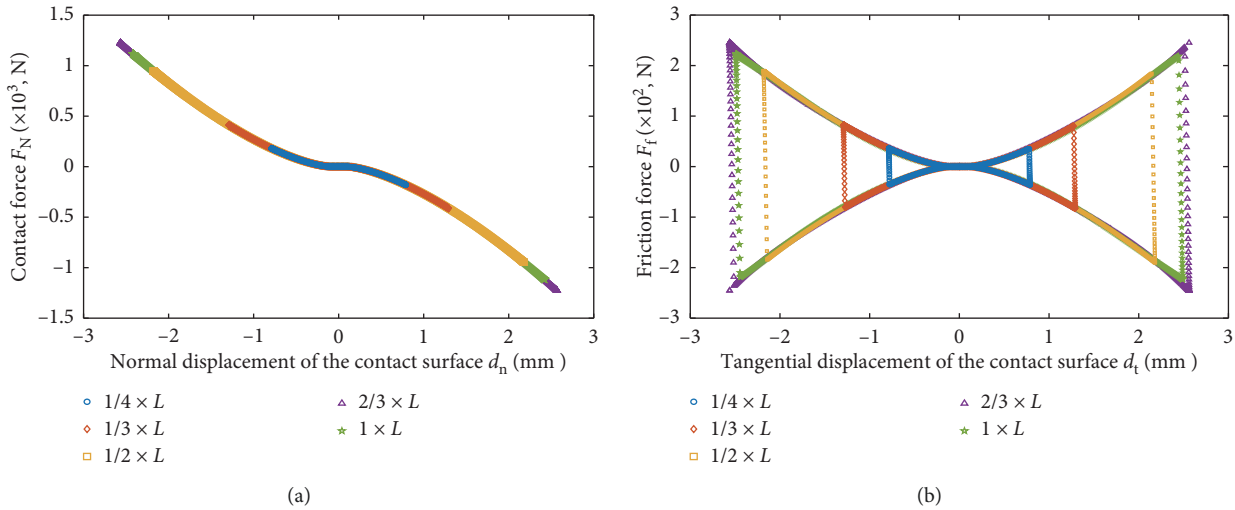

Figure 17: The curves of force at different shroud positions. (a) Contact forces. (b) Friction forces.

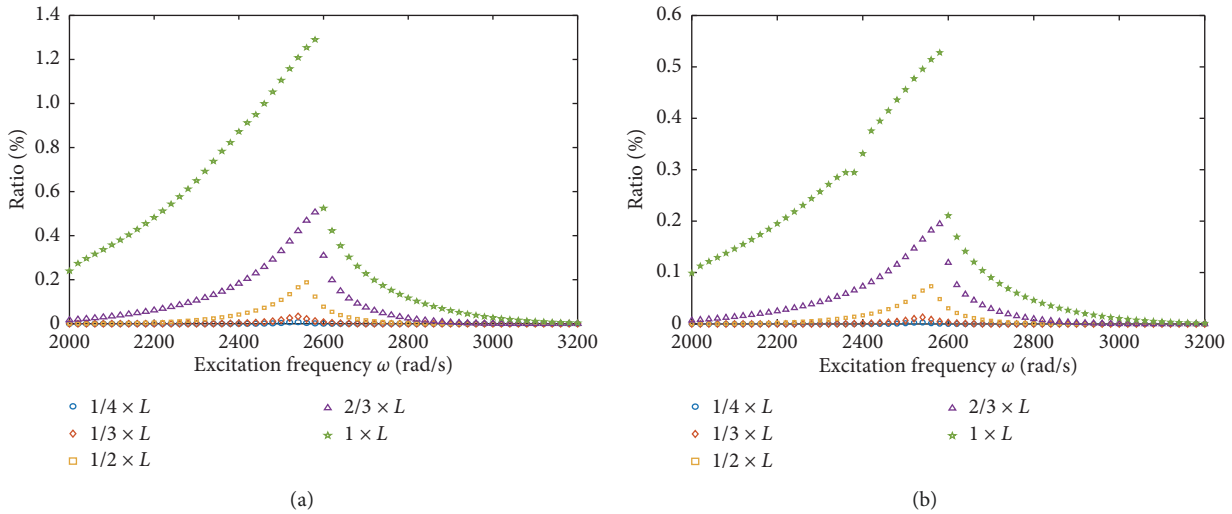

Figure 18: The energy ratio at different shroud positions. (a) The ratio of energy storage by the contact force. (b) The ratio of energy consumption by the friction force.

mechanism of the contact vibration of the flexible rotating shrouded blade is analyzed, and the effect of the rotational speed, contact angle, friction coefficient, clearance, and shroud position on the vibration response is investigated. Some conclusions can be summarized as follows:

(1) The amplitude-frequency curve of the shrouded blade exhibits a hard nonlinear phenomenon compared to the blade without shroud, and when vibrating, the resonance amplitude of the shrouded blade is lower, and the resonance frequency is larger, indicating that the introduction of the shroud brings a good vibration damping effect.

(2) In the parameters studied, since the centrifugal stiffening effect, when the rotational speed is increased, the resonance frequency of the blade also increases. When the contact angle becomes large, the resonance frequency increases, and the resonance amplitude decreases; however, when the contact angle reaches 60°, the resonance amplitude increases. As the coefficient of friction increases, the resonance amplitude decreases. And when the clearance is reduced or the shroud position is raised, the resonance amplitude is decreased while the resonance frequency is increased.

(3) In the studied parameter, the energy storage ratio of the contact force is always higher than the energy consumption ratio of the friction force, and only when the friction coefficient is taken as 0.5, the ratio of those two is relatively close. It shows that the contribution of contact force is more obvious than that of friction when the shroud shows the damping effect.

Appendix

Matrix Elements and Vectors Related to the Shrouded Blade

(1) The generalized coordinates vector $\boldsymbol{X}$:

$$\mathbf{X} = \left[q_{u1}(t) \dots q_{ui}(t) \dots q_{un}(t), q_{v1}(t) \dots q_{vi}(t) \dots q_{vn}(t), q_{w1}(t) \dots q_{wi}(t) \dots q_{wn}(t)\right]^{T}. \quad (A.1)$$

(2) Mass matrix of the shrouded blade $\mathbf{M}$:

$$\mathbf{M} = \begin{bmatrix} \mathbf{M}_1 & 0 & 0 \\ 0 & \mathbf{M}_2 & 0 \\ 0 & 0 & \mathbf{M}_3 \end{bmatrix}, \quad (A.2)$$

where $\mathbf{M}_1(i,j) = \rho A \int_0^L \varphi_i(x)\varphi_j(x)dx + m_s\varphi_i(\tilde{L})\varphi_j(\tilde{L})$, $\mathbf{M}_2(i,j) = \rho A \int_0^L \phi_i(x)\phi_j(x)dx + m_s\phi_i(\tilde{L})\phi_j(\tilde{L})$, $\mathbf{M}_3(i,j) = \rho A \int_0^L \eta_i(x)\eta_j(x)dx + m_s\eta_i(\tilde{L})\eta_j(\tilde{L})$, $i, j = 1, 2, \dots, n$.

(3) Coriolis matrix $\mathbf{G}$:

$$\mathbf{G} = \begin{bmatrix} 0 & \mathbf{G}_1 & 0 \\ \mathbf{G}_2 & 0 & 0 \\ 0 & 0 & 0 \end{bmatrix}, \quad (A.3)$$

where $\mathbf{G}_1(i,j) = 2\rho A\dot{\vartheta}\int_0^L \varphi_i(x)\phi_j(x)dx + 2m_s\dot{\vartheta}\varphi_i(\tilde{L})\phi_j(\tilde{L})$, $\mathbf{G}_2(i,j) = -2\rho A\dot{\vartheta}\int_0^L \phi_i(x)\varphi_j(x)dx - 2m_s\dot{\vartheta}\phi_i(\tilde{L})\varphi_j(\tilde{L})$, $i, j = 1, 2, \dots, n$.

(4) Structural stiffness matrix $\mathbf{K}_b$:

$$\mathbf{K}_b = \begin{bmatrix} \mathbf{K}_{b1} & 0 & 0 \\ 0 & \mathbf{K}_{b2} & 0 \\ 0 & 0 & \mathbf{K}_{b3} \end{bmatrix}, \quad (A.4)$$

where $\mathbf{K}_{b1}(i,j) = EA\int_0^L \varphi_i'(x)\varphi_j'(x)dx$, $\mathbf{K}_{b2}(i,j) = EI_z\int_0^L \phi_i''(x)\phi_j''(x)dx$, $\mathbf{K}_{b3}(i,j) = EI_y\int_0^L \eta_i''(x)\eta_\varphi''(x)dx$, $i, j = 1, 2, \dots, n$.

(5) Centrifugal stiffening matrix $\mathbf{K}_c$:

$$\mathbf{K}_c = \begin{bmatrix} 0 & 0 & 0 \\ 0 & \mathbf{K}_{c1} & 0 \\ 0 & 0 & \mathbf{K}_{c2} \end{bmatrix}, \quad (A.5)$$

where $\mathbf{K}_{c1}(i,j) = (1/2)\rho A\dot{\vartheta}^2[\int_0^{\tilde{L}} f_c(x)\phi_i'(x)\phi_j'(x)dx + \int_{\tilde{L}}^L f_c(x)\phi_i'(x)\phi_j'(x)dx]$, $\mathbf{K}_{c2}(i,j) = 1/2\rho A\dot{\vartheta}^2[\int_0^{\tilde{L}} f_c(x)\eta_i'(x)\eta_j'(x)dx + \int_{\tilde{L}}^L f_c(x)\eta_i'(x)\eta_j'(x)dx]$, $i, j = 1, 2, \dots, n$.

(6) Spin softening matrix $\boldsymbol{K}_s$:

$$\mathbf{K}_s = \begin{bmatrix} \mathbf{K}_{s1} & 0 & 0 \\ 0 & \mathbf{K}_{s2} & 0 \\ 0 & 0 & 0 \end{bmatrix}, \quad (A.6)$$

where $\mathbf{K}_{s1}(i,j) = -\rho A\int_0^L \varphi_i(x)\varphi_j(x)dx - m_s\varphi_i(\tilde{L})\varphi_j(\tilde{L})$, $\mathbf{K}_{s2}(i,j) = -\rho A\int_0^L \phi_i(x)\phi_j(x)dx - m_s\phi_i(\tilde{L})\phi_j(\tilde{L})$, $i, j = 1, 2, \dots, n$.

(7) Canonical external force vector $\boldsymbol{F}$:

$$\mathbf{F} = \begin{bmatrix} 0 \\ \mathbf{F}_1 \\ \mathbf{F}_2 \end{bmatrix}, \quad (A.7)$$

where $\mathbf{F}_1(i,1) = \phi_i(L/2)F_0\sin(\omega t) + \phi_i(\tilde{L})(F_N^l + F_N^r)\sin\theta + \phi_i(\tilde{L})(F_f^l + F_f^r)\cos\theta$, $\mathbf{F}_2(i,1) = \eta_i(L/2)\ F_0\sin(\omega t) - \eta_i(\tilde{L})(F_N^l + F_N^r)\cos\theta + \eta_i(\tilde{L})(F_f^l + F_f^r)\sin\theta$, $i = 1, 2, \dots, n$.

Nomenclature

$\mathbf{A}_1$:	Transformation matrix of the local coordinate system to the global coordinate system
A:	Cross-sectional area of the blade
B:	Blade width
$\mathbf{C}$:	Rayleigh damping matrix
d_t^l, d_t^r:	Tangential displacement of the left and right shroud
d_n^l, d_n^r:	Normal displacement of the left and right shroud
d_t, d_n:	Displacement of shrouded blade along the tangential and normal direction of the contact surface
E:	Young's modulus
E_F:	Elastic potential energy stored by the contact force in a single motion cycle
$\mathbf{F}$:	External force vector
F_N, F_f:	Total contact force and friction force
F_N^l, F_N^r:	Contact force of the left-side and right-side shroud
F_f^l, F_f^r:	Friction force of the left-side and right-side shroud
F_0:	Excitation amplitude
$f_c(x)$:	Centrifugal force and the expression
f_{n1}, f_{n2}, f_{n3}:	First three orders of bending frequencies
$\mathbf{G}$:	Coriolis force matrix
H:	Blade thickness
I_y, I_z:	Area moment of inertias about y and z axes of the blade section
$\mathbf{K}_b, \mathbf{K}_c, \mathbf{K}_s$:	Structural stiffness matrix, centrifugal stiffening matrix, and spin softening matrix
k_h:	Contact stiffness
k_t:	Shear stiffness of friction model
L:	Blade length
$\tilde{L}$:	Shroud position
$\mathbf{M}$:	Mass matrix
m_s:	Shroud mass
N:	Number of modal truncations
$q_{ui}(t), q_{vi}(t), q_{wi}(t)$:	Generalized coordinates
R_d:	Radius of the disk

$\mathbf{r}_{Q0}$, $\mathbf{r}_{s0}$: Position vector of an arbitrary point and shroud in local coordinate
$\mathbf{r}_Q$, $\mathbf{r}_s$: Displacement vector of an arbitrary point and shroud in global coordinate
T, T_b, T_s: Total kinetic energy of shrouded blade and kinetic energy of blade and shroud
U: Total potential energy of shrouded blade
u, $u_L^{\sim}$: Radial displacement of arbitrary point Q and shroud
$\mathbf{v}_Q$, $\mathbf{v}_s$: Velocity of arbitrary point Q and shroud
v, $v_L^{\sim}$: Flexural displacement of arbitrary point Q and shroud
w, $w_L^{\rightarrow}$: Swing displacement of arbitrary point Q and shroud
w_l, w_r: Displacement of frictional damper of the left-side and right-side contact surface
$\dot{w}_l$, $\dot{w}_r$: Velocity of frictional damper of the left-side and right-side contact surface
$\mathbf{X}, \dot{\mathbf{X}}, \ddot{\mathbf{X}}$: Generalized displacement, velocity, and acceleration vectors
$(\cdot)$: d/dt
α: Contact angle
δ: Shroud clearance
$\boldsymbol{\delta}_Q$, $\boldsymbol{\delta}_s$: Displacement vector of an arbitrary point and shroud in local coordinate
λ_i: Eigenvalue of the ith mode shape function
μ: Coefficient of friction
υ: Poisson's ratio
ρ: Blade density
ω: External excitation frequency
ω_1, ω_2: First- and second-order circular frequency of blade
Ω: Rotation speed of blade
ϑ: Angle between local coordinate and global coordinate
Δm: Mass of arbitrary point Q
$\varphi_i(x)$, $\phi_i(x)$, $\eta_i(x)$: ith modal shape functions in radial, flexural, and swing directions.

Data Availability

The data used to support the findings of this study are available from the corresponding author upon request.

Conflicts of Interest

The authors declare that they have no conflicts of interest.

Acknowledgments

This project was supported by the National Natural Science Foundation of China (no. 51575093) and the Fundamental Research Funds for the Central Universities (nos. N180313008, N170308028, and N170302001).

References

[1] Y. Kaneko, K. Mori, and H. Ohyama, "Development and verification of 3000 rpm 48 inch integral shroud blade for steam turbine," in *Proceedings of the ASME 2005 Power Conference*, pp. 609–616, American Society of Mechanical Engineers (ASME), Chicago, IL, USA, April 2005.

[2] K. Popp, L. Panning, and W. Sextro, "Vibration damping by friction forces: theory and applications," *Modal Analysis*, vol. 9, no. 3-4, pp. 419–448, 2016.

[3] A. A. Ferri and W. E. Whiteman, "Free response of a system with negative viscous damping and displacement-dependent dry friction damping," *Journal of Sound and Vibration*, vol. 306, no. 3–5, pp. 400–418, 2007.

[4] M. Allara, "A model for the characterization of friction contacts in turbine blades," *Journal of Sound and Vibration*, vol. 320, no. 3, pp. 527–544, 2009.

[5] C. H. Menq and B. D. Yang, "Non-linear spring resistance and friction damping of frictional constraint having two-dimensional motion," *Journal of Sound and Vibration*, vol. 217, no. 1, pp. 127–143, 1998.

[6] C.-H. Menq, P. Chidamparam, and J. H. Griffin, "Friction damping of two-dimensional motion and its application in vibration control," *Journal of Sound and Vibration*, vol. 144, no. 3, pp. 427–447, 1991.

[7] A. Muszynska and D. I. Jones, "Bladed disk dynamics investigated by a discrete model: effects of traveling wave excitation friction and mistuning," in *Proceedings of the Machinery Vibration Monitoring and Analysis Meeting*, pp. 33–49, Oak Brook, IL, USA, March-April1982.

[8] G. Nan and X. Ren, "Nonlinear dynamic analysis of shrouded turbine blade of aero-engine subjected to combination effect of impact and friction," in *Proceedings of the 2011 UkSim 13th International Conference on Computer Modelling and Simulation (UKSim)*, pp. 212–217, IEEE, Cambridge, UK, January 2011.

[9] B. He, H. Ouyang, S. He, X. Ren, and Y. Mei, "Dynamic analysis of integrally shrouded group blades with rubbing and impact," *Nonlinear Dynamics*, vol. 92, no. 4, pp. 2159–2175, 2018.

[10] M. Machado, P. Moreira, P. Flores, and H. M. Lankarani, "Compliant contact force models in multibody dynamics: evolution of the Hertz contact theory," *Mechanism and Machine Theory*, vol. 53, pp. 99–121, 2012.

[11] S. Bab, S. E. Khadem, A. Abbasi, and M. Shahgholi, "Dynamic stability and nonlinear vibration analysis of a rotor system with flexible/rigid blades," *Mechanism and Machine Theory*, vol. 105, pp. 633–653, 2016.

[12] S.-T. Choi and Y.-T. Chou, "Vibration analysis of elastically supported turbomachinery blades by the modified differential quadrature method," *Journal of Sound and Vibration*, vol. 240, no. 5, pp. 937–953, 2001.

[13] J. Szwedowicz, R. Visser, W. Sextro, and P. A. Masserey, "On nonlinear forced vibration of shrouded turbine blades," *Journal of Turbomachinery*, vol. 130, no. 1, p. 011002, 2008.

[14] D. Cao, X. Gong, D. Wei, S. Chu, and L. Wang, "Nonlinear vibration characteristics of a flexible blade with friction damping due to tip-rub," *Shock and Vibration*, vol. 18, no. 1-2, pp. 105–114, 2011.

[15] L. H. Cao, J. X. Wang, P. Li, P. F. Hu, and Y. Li, "Numerical analysis on steam exciting force caused by rotor eccentricity," *Shock and Vibration*, vol. 2017, Article ID 8602965, 9 pages, 2017.

[16] S. Chu, D. Cao, S. Sun, J. Pan, and L. Wang, "Impact vibration characteristics of a shrouded blade with asymmetric gaps under wake flow excitations," *Nonlinear Dynamics*, vol. 72, no. 3, pp. 539–554, 2013.

[17] G. Nan, "Modeling and dynamic analysis of shrouded turbine blades in aero-engines," *Journal of Aerospace Engineering*, vol. 29, article 04015021, 2015.

[18] H. Ma, F. Xie, H. Nai, and B. Wen, "Vibration characteristics analysis of rotating shrouded blades with impacts," *Journal of Sound and Vibration*, vol. 378, pp. 92–108, 2016.

[19] F. Xie, H. Ma, C. Cui, and B. Wen, "Vibration response comparison of twisted shrouded blades using different impact models," *Journal of Sound and Vibration*, vol. 397, pp. 171–191, 2017.

[20] M.-R. Ghazavi, A. Najafi, and A.-A. Jafari, "Bifurcation and nonlinear analysis of nonconservative interaction between rotor and blade row," *Mechanism and Machine Theory*, vol. 65, pp. 29–45, 2013.

[21] E. Petrov, "Method for direct parametric analysis of nonlinear forced response of bladed discs with friction contact interfaces," in *Proceedings of the ASME Turbo Expo 2004: Power for Land, Sea, and Air*, pp. 397–408, American Society of Mechanical Engineers (ASME), Vienna, Austria, June 2004.

[22] W. Gu and Z. Xu, "3D numerical friction contact model and its application to nonlinear blade damping," in *Proceedings of the ASME Turbo Expo 2010: Power for Land, Sea, and Air*, pp. 809–817, American Society of Mechanical Engineers (ASME), Glasgow, UK, June 2010.

[23] W. Gu, Z. Xu, and S. Wang, "Advanced modelling of frictional contact in three-dimensional motion when analysing the forced response of a shrouded blade," *Proceedings of the Institution of Mechanical Engineers, Part A: Journal of Power and Energy*, vol. 224, no. 4, pp. 573–582, 2010.

[24] W. Gu, Z. Xu, and Y. Liu, "A method to predict the non-linear vibratory response of bladed disc system with shrouded dampers," *Proceedings of the Institution of Mechanical Engineers, Part C: Journal of Mechanical Engineering Science*, vol. 226, no. 6, pp. 1620–1632, 2012.

[25] S. Zucca, M. M. Gola, and F. Piraccini, "Non-linear dynamics of steam turbine blades with shroud: numerical analysis and experiments," in *Proceedings of the ASME Turbo Expo 2012: Turbine Technical Conference and Exposition*, pp. 665–674, American Society of Mechanical Engineers (ASME), Copenhagen, Denmark, June 2012.

[26] Y. Liu, B. Shangguan, and Z. Xu, "A friction contact stiffness model of fractal geometry in forced response analysis of a shrouded blade," *Nonlinear Dynamics*, vol. 70, no. 3, pp. 2247–2257, 2012.

[27] Y. Liu, S. Bo, and Z. Xu, "Improved hybrid frequency-time domain method for nonlinear analysis of frictionally damped blade systems," in *Proceedings of the ASME Turbo Expo 2016: Turbomachinery Technical Conference and Exposition*, American Society of Mechanical Engineers (ASME), Coex, Seoul, Korea, June 2016.

[28] E. B. Hunt and F. Crossley, "Review and prospectus," *Artificial Intelligence*, vol. 42, pp. 440–445, 1975.